


Interaction effects in graphene in a weak magnetic field

Ke Wang^{1,*}, M. E. Raikh,² and T. A. Sedrakyan^{1,†}

¹*Department of Physics, University of Massachusetts, Amherst, Massachusetts 01003, USA*

²*Department of Physics and Astronomy, University of Utah, Salt Lake City, Utah 84112, USA*

 (Received 26 June 2021; revised 18 August 2021; accepted 27 September 2021; published 4 October 2021)

A weak perpendicular magnetic field, B , breaks the chiral symmetry of each valley in the electron spectrum of graphene, preserving the overall chiral symmetry in the Brillouin zone. We explore the consequences of this symmetry breaking for the interaction effects in graphene. In particular, we demonstrate that the electron-electron interaction lifetime acquires an anomalous B dependence. Also, the ballistic zero-bias anomaly, $\delta\nu(\omega)$, where ω is the energy measured from the Fermi level, emerges at a weak B and has the form $\delta\nu(B) \sim B^2/\omega^2$. Temperature dependence of the magnetic-field corrections to the thermodynamic characteristics of graphene is also anomalous. We discuss experimental manifestations of the effects predicted. The microscopic origin of the B -field sensitivity is an extra phase acquired by the electron wave function resulting from the chirality-induced pseudospin precession.

DOI: [10.1103/PhysRevB.104.L161102](https://doi.org/10.1103/PhysRevB.104.L161102)

Introduction. Electron spectrum in graphene possesses a chiral (pseudospin) structure [1,2]. Two pseudospin projections are identified with two points, K and K' , of the Brillouin zone near which the spectrum is characterized by a massless Dirac dispersion. Numerous consequences of the Dirac spectrum of graphene for the disorder and interaction effects were established (see, e.g., Refs. [3–20]).

One distinctive feature of the graphene band structure is the absence of backscattering from the impurities. This feature is a consequence of orthogonality of the spinors corresponding to the wave vectors \mathbf{k} and $-\mathbf{k}$. In turn, the absence of backscattering leads to the suppression of the oscillations of electron density (Friedel oscillations [21]) created by an impurity in graphene [22,23]. In the ballistic regime [24–27], electron scattering from individual impurities dressed by the Friedel oscillations is responsible for a zero-bias anomaly $\propto \ln\omega$ in conventional two-dimensional (2D) electron gas. Here ω is the energy measured from the Fermi level and the condition $\omega\tau \gg 1$, where τ is the elastic scattering time, is implied. Fast decay of the Friedel oscillations suggests that zero-bias anomaly in graphene is absent [23,28]. A more detailed study [29] indicated that it is the Hartree correction which is absent in graphene, while the Fock correction, originating from the forward scattering, is still present.

In the absence of impurities, electron-electron interactions in 2D electron gas cause nonanalytic corrections [30–33] to the self-energy, $\Sigma(\omega)$. At low temperatures, $T \ll \omega$, the imaginary part of self-energy has the form $\tau_{ee}(\omega)^{-1} \sim (\omega^2/E_F)\ln(E_F/\omega)$, where E_F is the Fermi energy. Correspondingly, the real part of self-energy behaves as $\text{Re}\Sigma(\omega) \sim \omega^2\text{sgn}(\omega)$. At finite T , interactions cause a correction to the specific heat [34,35] $\delta C(T) \propto T^2$. Microscopically, the above

corrections emerge in the random-phase approximation. Their derivation is so general that it is natural to expect that, in doped graphene, the interaction corrections have the same Fermi-liquid form [36].

In the present Letter, we identify the interaction effects specific to graphene. These effects emerge in the presence of a weak magnetic field. Their origin is the field-induced lifting of chiral symmetry in K and K' valleys of graphene while preserving the overall symmetry. To capture these effects, one should go beyond the random-phase approximation.

With regard to ballistic zero-bias anomaly, lifting of the chiral symmetry in the field, B , gives rise to the contribution $\propto B^2/\omega^2$, which can be even *stronger* than the zero-field contribution [29]. A formal difference between the calculations of the ballistic zero-bias anomaly in electron gas with parabolic spectrum and in graphene is that the Green's functions, which enter into the calculation, have a matrix structure in graphene. Without this matrix structure, the B -sensitive contributions to the tunnel conductance *cancel out*.

A natural energy scale imposed by the field, B , in graphene is $\omega_0 = v_F/R_L$, where $R_L \propto B^{-1}$ is the Larmor radius. Quantization of the energy levels can be neglected for $\omega \gg \omega_0$. We show that the B -dependent correction to the thermodynamic characteristics of the clean graphene can be conveniently expressed in terms of ω_0 . Namely, the corrections to the imaginary and real parts of self-energy behave as $\text{Im}[\Sigma(\omega, B) - \Sigma(\omega, 0)] \sim \omega_0^2 E_F^{-1} \ln(\omega/T)$ and $\text{Re}[\Sigma(\omega, B) - \Sigma(\omega, 0)] \sim \omega_0^2 E_F^{-1} \text{sgn}(\omega)$, respectively. On the basis of these results we draw the consequences for observables. Namely, we show that the B -dependent correction to the specific heat is temperature independent in a wide temperature interval.

Electrons in a weak magnetic field. The Hamiltonian of monolayer graphene which incorporates the B field in the Landau gauge reads

$$\hat{H}_B = v_F[(p_x - eBy)\hat{\Sigma}_x + p_y\hat{\Sigma}_y]. \quad (1)$$

*kewang@umass.edu

†tsedrakyan@umass.edu

Here v_F is the Fermi velocity. Here $\hat{r} = \mathbf{r}/r$, $\Sigma = (\Sigma_x, \Sigma_y)$ and $\Sigma_x = \hat{t}_z \otimes \hat{\sigma}_x$, $\Sigma_y = \hat{t}_z \otimes \hat{\sigma}_y$. The Pauli matrices $\hat{\sigma}_i$ act in the space of A and B sublattices of the honeycomb lattice and \hat{t} is the Pauli matrix distinguishing between two Dirac points in graphene. Diagonalizing the Hamiltonian, one finds that the linear spectrum is transformed into a nonuniform ladder of spectrum, $\sqrt{2nv_F/l}$. Here $n \geq 0$ and $l = \sqrt{\hbar/eB}$ is the magnetic length. Under a weak field, the spectrum around the Fermi level, E_F , can be linearized as $\sqrt{2nv_F/l} \simeq E_F + (n - N_F)v_F(k_F l^2)^{-1}$, where $N_F = (k_F l^2)^2/2$. This yields the expression for the effective cyclotron frequency $\omega_0 = v_F(k_F l^2)^{-1}$.

The Feynman propagator of free Dirac electrons is known to possess a nontrivial matrix structure. Namely, in the absence of magnetic field, the propagator in the real space is given by [29]

$$G_\omega(\mathbf{r}) = \frac{k_F}{2v_F} \sqrt{\frac{1}{2k_F r}} e^{i \text{sgn}(\omega)\Phi_0(r)} M_0, \quad (2)$$

where the phase $\Phi_0(r) = k_F r + \omega r/v_F + \pi/4$ and the matrix M_0 is given by $M_0 = [\text{sgn}(\omega) + i(2k_F r)^{-1}] \hat{r} \cdot \Sigma + \hat{I}$. Here $\hat{r} = \mathbf{r}/r$, $\Sigma = (\Sigma_x, \Sigma_y)$, and \hat{I} is the identity matrix. This matrix structure reflects the chiral symmetry of electrons: fast decay of the Friedel oscillations [23] and the absence of a zero-bias anomaly [29] are the consequences of this matrix form.

The presence of magnetic field modifies the gauge-invariant part of the electron propagator by breaking the chiral symmetry of the electrons in the vicinity of the Dirac point.

Field-induced modification of Eq. (2) amounts to the changes of $\Phi_0(r)$ and $M_0(r)$. The phase Φ_0 becomes $\Phi = \Phi_0 - r^3/(24k_F l^4)$, which is due to the curving of the semiclassical trajectory [37–39] in a weak field. In graphene, due to the matrix structure of the Hamiltonian, the identity matrix \hat{I} in M_0 transforms into a new four-dimensional field-dependent matrix. This matrix contains $\hat{\Sigma}_z$, and thus, does not commute with M_0 . This is because M_0 contains the matrices $\hat{\Sigma}_{x,y}$. Here $\hat{\Sigma}_z = \hat{\sigma}_z \otimes \hat{\tau}_0$, where τ_0 is a 2×2 unit matrix.

Specific form of the matrix, M , is the following:

$$M[\mathbf{r}, \text{sgn}(\omega)] \simeq M_0 - i \text{sgn}(\omega)\varphi(r)\hat{\Sigma}_z - \frac{\varphi(r)^2}{2}\hat{I}, \quad (3)$$

where $\varphi(r) = \omega_0 r/(2v_F)$ is half of the angle corresponding to the arc of the Larmor circle with length r . Equation (3) applies in the domain $k_F^{-1} < r < k_F l^2 = R_L$.

The *pseudospin* structure of the term $\sim \varphi(r)\hat{\Sigma}_z$ in the propagator, while preserving the chiral symmetry of the system [1,40], reflects the field-induced breaking thereof around a single Dirac cone (see Fig. 1 for a graphical representation of this effect).

In general, the ballistic correction to the density of states is given by two diagrams shown in Figs. 2(a) and 2(b), which provide comparable contributions. However, as shown in Ref. [29], in graphene the Fock diagram dominates over the Hartree diagram in the absence of magnetic field. This is a consequence of the suppressed backscattering. We show [42] that the weak magnetic field does not change the picture, namely, the Fock diagram is still dominating. We will thus focus on the sensitivity of the Fock diagram to a weak magnetic field.

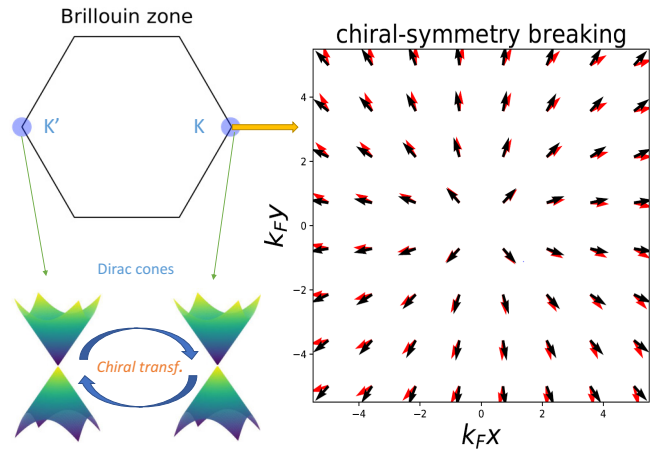


FIG. 1. The left panel depicts the Brillouin zone of graphene. Around the K and K' valleys, the spectrum is Dirac-like, supporting low-energy Hamiltonians \hat{H}_K and $\hat{H}_{K'}$ that are connected via a chiral transformation, $H_K = \hat{\sigma}_z H_{K'} \hat{\sigma}_z$. The right panel depicts the vector field $\mathbf{v}_K(\mathbf{r})$ (for definition, see Ref. [41]), at K valley. The dark (black) vectors field represents the $\mathbf{v}_K(\mathbf{r})$ at zero magnetic field. The gray (red) vector field is the $\mathbf{v}_K(\mathbf{r})$ at a weak but nonzero magnetic field. Here we take $\omega_0/(2E_F) = 0.07$. The figure shows the chiral symmetry of the state at $B = 0$. At finite B , the chiral symmetry in one valley is broken. In the leading approximation, the angle between two vector fields is proportional to $\varphi(r)$. Importantly, the chiral transformation leads to the relation $\mathbf{v}_K(\mathbf{r}) = \mathbf{v}_K(-\mathbf{r})$, manifesting the chiral symmetry of the whole system.

We start with a matrix generalization of the analytical expressions for the Fock diagram, Fig. 2(a). For this purpose, we consider a nonmagnetic impurity causing a perturbation $\hat{u}\delta(\mathbf{r})$ and the screened interaction potential, $U(\mathbf{r})$, with a radius

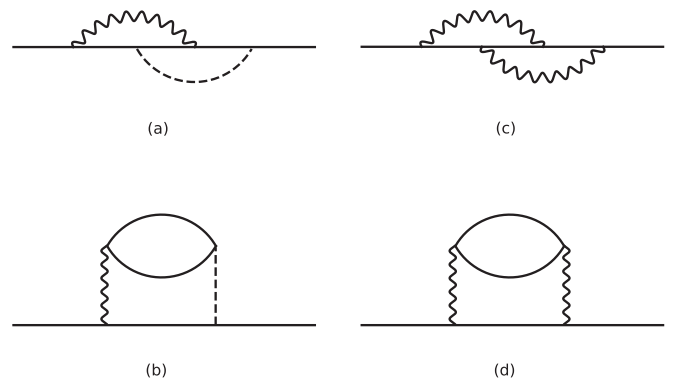


FIG. 2. Diagrams for the corrections to the Green's function. Solid lines represent the Feynman propagators. Wavy lines represent the electron-electron interactions. (a) represents the Fock diagram involving a single-impurity scattering. It yields a leading contribution to the B^2 ballistic zero-bias anomaly. (b) represents a Hartree diagram involving a single-impurity scattering. It is insensitive to a weak magnetic field. (c) and (d) represent, respectively, the Fock and Hartree diagrams for the B^2 correction to the electron lifetime. Unlike the Hartree diagram, which is the first diagram of the RPA sequence, diagram (c) yields an anomalous temperature dependence.

$\sim k_F^{-1}$. The corresponding expression reads

$$\delta G_\omega(\mathbf{r}, \mathbf{r}) = \int d\mathbf{r}_1 d\mathbf{r}_2 G_\omega(\mathbf{r}, \mathbf{r}_1) H_F(\mathbf{r}_1, \mathbf{r}_2) G_\omega(\mathbf{r}_2, \mathbf{0}) \times \hat{u} G_\omega(\mathbf{0}, \mathbf{r}) + (\hat{u} \leftrightarrow H_F). \quad (4)$$

Here G_ω is the free Feynman propagator of the Dirac electrons between the position of impurity $\mathbf{r} = 0$ and the point \mathbf{r} , while H_F stands for nonlocal Fock potential

$$H_F = \frac{i}{2\pi} \int d\Omega G_{\omega+\Omega}(\mathbf{r}_1, \mathbf{0}) \hat{u} G_{\omega+\Omega}(\mathbf{0}, \mathbf{r}_2) U(\mathbf{r}_1 - \mathbf{r}_2). \quad (5)$$

The interaction correction to the local density of states, $\delta v_\omega(\mathbf{r})$, is related to the retarded Green's function as $\delta v_\omega(\mathbf{r}) = -\frac{2}{\pi} \text{Tr} \text{Im} \delta G_\omega(\mathbf{r}, \mathbf{r})$.

The structure of Eqs. (4) and (5) suggests that $\delta v_\omega(\mathbf{r})$ contains the product of 4×4 matrices. In the semiclassical limit, all trajectories $\mathbf{r} \rightarrow \mathbf{r}_1 \rightarrow \mathbf{r}_2 \rightarrow \mathbf{0} \rightarrow \mathbf{r}$ contributing to δG are close to a straight line. With screened Coulomb potential being pointlike, the Fock diagram involves the following product of the M matrices:

$$F \equiv \text{tr}[\hat{u}M(\mathbf{r}, +)M(-\mathbf{r}, -)\hat{u}M(\mathbf{r}, -)M(-\mathbf{r}, +)]. \quad (6)$$

For a qualitative discussion, let us choose \hat{u} in the form of a scalar, $u_0 \hat{l}$. Then the leading field-dependent term emerges as a coefficient in front of the product of the projection operators $\text{tr}[\hat{\Sigma}_z \hat{\Sigma}_{x/y} \hat{\Sigma}_z \hat{\Sigma}_{x/y}]$. Since the term $\hat{\Sigma}_z$ appears in the matrix M in combination with $\varphi(r)$, we have $F \propto \varphi^2(r)$. With the help of the commutation relations for $\hat{\Sigma}_x$, $\hat{\Sigma}_y$, and $\hat{\Sigma}_z$, it is easy to check that $\text{tr}[\hat{\Sigma}_z \hat{\Sigma}_{x/y} \hat{\Sigma}_z \hat{\Sigma}_{x/y}] = -\text{tr}[I]$, i.e., it is nonzero. An estimate for F is $\sim u_0^2 \varphi^2(r) \sim u_0^2 \omega_0^2 r^2 / v_F^2$. With characteristic r being v_F / ω , this estimate translates into $u_0^2 \omega_0^2 / \omega^2$. Below we examine a number of observables having the structure similar to Eq. (4).

Emerging zero-bias anomaly. For the scalar impurity scattering, $\hat{u} = u_0 \hat{l}$, there is no zero-bias anomaly in graphene [29]. To convert the above estimate for F into the B -dependent correction to the density of states, we perform the spatial averaging of Eq. (4), which generates the impurity concentration, n_i . Final result reads

$$\frac{\delta v_\omega(B) - \delta v_\omega(0)}{v_F} \simeq \frac{\lambda_0 n_i u_0^2 \omega_0^2}{8\pi v_F^2 \omega^2}, \quad (7)$$

where $\lambda_0 = k_F U_0 / (2\pi v_F)$ stands for dimensionless interaction parameter, U_0 is the interaction potential with zero momentum transfer, and $v_F = k_F / (\pi v_F)$. The zero-bias anomaly is shown in Fig. 3 for various field strengths.

The most general form of the pointlike perturbation, \hat{u} , consistent with time-reversal symmetry is $\hat{u} = u_0 \hat{l} + \sum_{s,l=x,y,z} u_{sl} \Sigma_s \Lambda_l$. Here $\Lambda_{x,y} = \hat{\tau}_{x,y} \otimes \hat{\sigma}_z$, $\Lambda_z = \hat{\tau}_z \otimes \hat{\sigma}_0$. The remaining nine types of the disorder can be incorporated into Eq. (7) by replacing u_0^2 by $t = u_0^2 - \sum_l u_{il}^2$.

The result Eq. (7) was obtained under the assumptions $\omega\tau \gg 1$ and $\omega \gg \omega_0$ which ensure the ballistic regime and the irrelevance of the Landau quantization, respectively.

Emergence of a zero-bias anomaly in graphene in the presence of magnetic field manifests itself in the local density of states (DOS), $\delta v_\omega(\mathbf{r}, B) = -2\pi^{-1} \text{tr}[\text{Im} G_R(\mathbf{r}, \mathbf{r}, \omega)]$. Evalua-

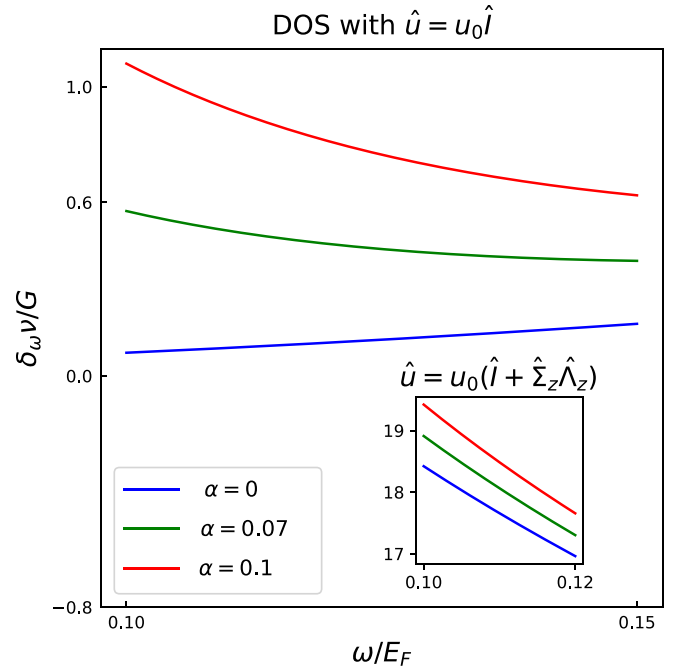


FIG. 3. Plot (a) and the inset illustrate the energy dependence of the interaction correction to the density of states. Three curves correspond to the three values of the dimensionless magnetic field $\alpha = (k_F l)^{-2}$. Plot (a) is for the scalar impurity with magnitude $\hat{u} = u_0 \hat{l}$. The correction, δv , is measured in units of $G = v_F n_i (u_0 / 2v_F)^2 \lambda_0 / 2\pi$. Note that for $\alpha = 0$ the zero-bias anomaly is absent, so that δv is a smooth function of energy, ω , measured from the Fermi level. In the low-energy regime, $\omega/E_F < \sqrt{\alpha}$, the B -dependent anomalous term in δv dominates and behaves as $\sim \alpha^2 E_F^2 / \omega^2$. The inset of plot (a) is for the impurity-induced perturbation. For this perturbation, zero-bias anomaly exists even in the absence of magnetic field. The magnetic contribution yields only a small correction to the logarithmic δv .

tion of Eq. (4) yields

$$\frac{\delta v_\omega(\mathbf{r}, B) - \delta v_\omega(\mathbf{r}, 0)}{v_F} \simeq \frac{\lambda_0 t \omega_0^2}{(2\pi v_F^2)^2} \cos \frac{\omega r}{v_F}. \quad (8)$$

Note that, unlike the $B = 0$ case [29], the interaction correction Eq. (8) is isotropic. The most dramatic difference between Eq. (8) and the $B = 0$ result is that the zero-field correction falls off as $1/r^2$, while the amplitude of oscillations in Eq. (8) does not depend on r . Naturally, the falloff starts from the distances $r \gtrsim R_L = v_F / \omega_0$, where Eq. (8) does not apply. Technically, the extra factor r^2 comes from $\varphi^2(r)$ in the factor F . In relation to the local DOS, we would like to point out that it can be measured experimentally using the scanning tunneling microscopy [43,44].

Quasiparticle lifetime. Energy dependence of electron-electron scattering rate, τ_{ee}^{-1} , in doped graphene is $\omega^2 \ln(E_F / \omega)$, as in a regular Fermi liquid [36]. This dependence emerges already in the lowest order of the perturbation theory. A corresponding diagram is illustrated in Fig. 2. Subsequent summation of the higher-order diagrams within the random-phase approximation (RPA) modifies the prefactor in τ_{ee}^{-1} . Equally, the calculations leading to nonanalytic interaction corrections [33] apply to the doped

graphene. With regard to the magnetic field dependence of τ_{ee}^{-1} , it appears that, similarly to the zero-bias anomaly, the leading B dependence originates from the Fock diagram on Fig. 2(c), which is beyond the RPA.

The result for the correction, $\delta\tau_{ee}^{-1}(B)$, depends on the ratio ω/T . In the low- T limit, $\omega \gg T$, this correction reads

$$\delta\tau_{ee}^{-1}(B) \simeq \frac{\lambda_0 \lambda_{2k_F} \omega_0^2}{2\pi E_F} \ln\left(\frac{|\omega|}{\Delta}\right), \quad |\omega| \gg T, \quad (9)$$

where $\lambda_{2k_F} = k_F U_{2k_F} / (2\pi v_F)$, $\Delta = \max\{T, \tau_{ee}^{-1}\}$. The relative magnitude of the correction is essentially $(\omega_0/\omega)^2$ and, similarly to the zero-bias anomaly, it originates from the magnetic phase $\hat{\Sigma}_z \varphi(r)$ of the propagator in Feynman diagrams.

In the high-temperature limit, $T \gg \omega$, evaluation of the B -dependent correction to the diagram Fig. 2(c) yields

$$\delta\tau_{ee}^{-1}(B) \simeq -\ln(2) \frac{\lambda_0 \lambda_{2k_F} \omega_0^2}{2\pi E_F}, \quad T \gg |\omega|. \quad (10)$$

Note that the correction is T independent, but it exists on the background of the T^2 main term.

Effective velocity and specific heat. In the doped graphene, as in 2D electron gas, the effective velocity of quasiparticles, v^* , and specific heat, C_v , are expected to acquire interaction corrections [33,36,42]. These corrections scale as $\delta v^* \propto T$ and $\delta C_v \propto T^2$, respectively. Both anomalies originate from the nonanalytic corrections to the quasiparticle lifetime [33]. Here we trace how the ω_0^2 corrections specific for graphene manifest themselves in v^* and C_v . The question of interest is the temperature dependence of these corrections. We found that the correction to v^* behaves as ω_0^2/T , while the correction to C_v is $\propto \omega_0^2/v_F^2$ and is T independent. Both originate from ω_0^2 correction to the lifetime given by Eqs. (9) and (10).

Another ingredient required to find the B -dependent corrections to v^* and C_v is the electron spectrum renormalized by the interactions. The corresponding ω_0^2 correction comes from the Fock diagram Fig. 2(c):

$$\begin{aligned} & \text{Re}[\Sigma(\omega, B) - \Sigma(\omega, 0)] \\ & \simeq -\frac{\lambda_0 \lambda_{2k_F} \omega_0^2}{16E_F} \begin{cases} \text{sgn}(\omega), & |\omega| \gg T \\ \omega/(2T), & |\omega| \ll T. \end{cases} \end{aligned} \quad (11)$$

The above correction can, in principle, be measured using the angle-resolved photoemission spectroscopy [45] from the analysis of the constant energy maps [46] at different values of B .

In the limit $T \gg \omega$, the renormalized spectrum Eq. (11) leads to the following correction to the effective velocity of quasiparticles $v = v_F / (1 - \partial_\omega \text{Re}\Sigma|_{\omega=0})$ [42]:

$$\frac{v(B) - v(0)}{v_F} \simeq -\frac{\lambda_0 \lambda_{2k_F} \omega_0^2 E_F}{32E_F^2 T}. \quad (12)$$

Note that $v(0)$ contains a nonmagnetic interaction correction which is linear in T . On the contrary, the B -dependent correction is $\propto T^{-1}$. This feature is illustrated in Fig. 4 for several values of B . Since the thermodynamical potential, Ω , involves the summation over energies of quasiparticles near the Fermi level, the energy correction in Eq. (11) has nontrivial implications for thermodynamics. Here we consider the specific heat per unit volume, $C_v = V^{-1} \partial \Omega / \partial T$, where V is the volume of

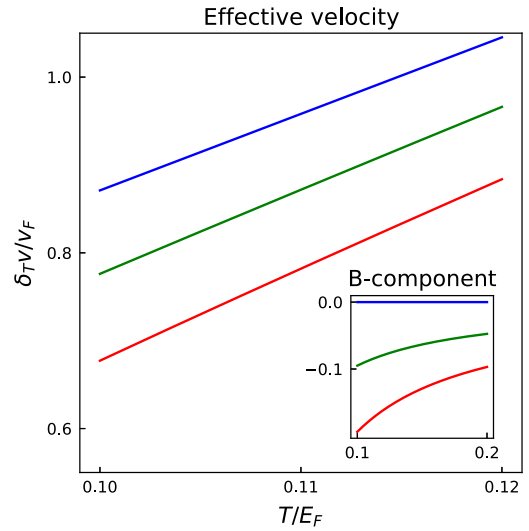


FIG. 4. In the plot the temperature-dependent interaction correction to the effective velocity, $\delta_T v^* = v_T^*(B) - v_{T=0}^*(B)$, is shown. The inset shows the B -dependent component of the effective velocity, $\delta_T v^*(B) - \delta_T v^*(0)$. This part behaves as an inverse temperature, $\sim \alpha^2 E_F / T$.

system. The result for specific heat [42] in the limit $T \gg \omega_0$ is the following:

$$\delta C_v(B) - \delta C_v(0) \simeq -\frac{\lambda_0 \lambda_{2k_F} \omega_0^2}{8\pi v_F^2}, \quad (13)$$

where $\delta C_v(B)$ is the interaction correction to the specific heat. Note that $\delta C_v(0)$ contains the conventional T^2 term, specific for 2D Fermi liquid. We find that the field-dependent correction to δC_v is a T independent. In the absence of electron-phonon interactions, the field-dependent correction exists in a parametrically large interval of temperatures, $\omega_0 < T < E_F$. Equation (13) can be verified experimentally by measuring the specific heat of graphene in a comprehensive Raman optothermal method [47].

Conclusion. Our main finding is that, for two-dimensional Dirac electrons, application of a weak magnetic field enhances significantly the many-body effects. This is unlike the conventional 2D electron gas. The reason for this is the pseudospin-dependent magnetic correction in Dirac electron propagators, $\sim \Sigma_z \varphi(r)$. For many-body effects to unfold, the energy, ω , measured from the Fermi level should exceed $\omega_0 = v_F (k_F l^2)^{-1}$, which is the inter-Landau-level distance at the Fermi level. We have only considered the low-temperature properties of interacting electrons in the doped graphene, so that the interaction with phonons [48,49] can be neglected.

Our predictions for observables given by Eqs. (9)–(13) and by Eq. (7) all emerge as a result of evaluation of the Fock diagrams illustrated in Figs. 2(a) and 2(c). It is nontrivial that, while these diagrams are not leading and even do not belong to the RPA sequence, they are responsible for the sensitivity to a weak magnetic field. Importantly, the higher-order diagrams, while leading to the renormalization of the interaction vertex, do not modify the predicted ω, T dependencies.

Another origin of the B dependence of the interaction effects is either spin via the Zeeman splitting coming from

spin or the orbital effect via the curving of the electron trajectories in magnetic field. We have checked [42] that these two mechanisms lead to the B -dependent corrections which are subleading compared to those originating from the pseudospin-dependent phase of Dirac propagators.

Finally, we emphasize that our results apply for the doped graphene, where the Fermi energy is far away

from the neutrality. The condition $\omega \gg \omega_0$ in the present Letter is automatically violated at neutrality. The question about $\nu = 0$ Landau level is interesting and remains open [50,51].

Acknowledgments. The research was supported by startup funds from the University of Massachusetts, Amherst (K.W. and T.A.S.) and by the Department of Energy, Office of Basic Energy Sciences, Grant No. DE-FG02-06ER46313 (M.E.R.).

-
- [1] G. W. Semenoff, Condensed-Matter Simulation of a Three-Dimensional Anomaly, *Phys. Rev. Lett.* **53**, 2449 (1984).
- [2] M. I. Katsnelson, K. S. Novoselov, and A. K. Geim, Chiral tunnelling and the Klein paradox in graphene, *Nat. Phys.* **2**, 620 (2006).
- [3] A. Altland, Low-Energy Theory of Disordered Graphene, *Phys. Rev. Lett.* **97**, 236802 (2006).
- [4] I. L. Aleiner and K. B. Efetov, Effect of Disorder on Transport in Graphene, *Phys. Rev. Lett.* **97**, 236801 (2006).
- [5] W. K. Tse, Ben Yu-Kuang Hu, and S. Das Sarma, Chirality-Induced Dynamic Kohn Anomalies in Graphene, *Phys. Rev. Lett.* **101**, 066401 (2008).
- [6] A. H. Castro Neto, F. Guinea, N. M. R. Peres, K. S. Novoselov, and A. K. Geim, The electronic properties of graphene, *Rev. Mod. Phys.* **81**, 109 (2009).
- [7] S. Das Sarma, S. Adam, E. H. Hwang, and E. Rossi, Electronic transport in two-dimensional graphene, *Rev. Mod. Phys.* **83**, 407 (2011).
- [8] V. N. Kotov, B. Uchoa, V. M. Pereira, F. Guinea, and A. H. Castro Neto, Electron-electron interactions in graphene: Current status and perspectives, *Rev. Mod. Phys.* **84**, 1067 (2012).
- [9] G. W. Semenoff, Chiral symmetry breaking in graphene, *Phys. Scr.* **T146**, 014016 (2012).
- [10] R. Nandkishore, L. S. Levitov, and A. V. Chubukov, Chiral superconductivity from repulsive interactions in doped graphene, *Nat. Phys.* **8**, 158 (2012).
- [11] C. Dutreix, H. González-Herrero, I. Brihuega, M. I. Katsnelson, C. Chapelier, and V. T. Renard, Measuring the Berry phase of graphene from wavefront dislocations in Friedel oscillations, *Nature (London)* **574**, 219 (2019).
- [12] M. Agarwal and E. G. Mishchenko, Dynamic response functions of two-dimensional Dirac fermions with screened Coulomb and short-range interactions, *Phys. Rev. B* **102**, 125421 (2020).
- [13] S. Maiti and T. A. Sedrakyan, Composite fermion state of graphene as a Haldane-Chern insulator, *Phys. Rev. B* **100**, 125428 (2019).
- [14] J. Pack, B. J. Russell, Y. Kapoor, J. Balgley, J. Ahlers, T. Taniguchi, K. Watanabe, and E. A. Henriksen, Broken Symmetries and Kohn's Theorem in Graphene Cyclotron Resonance, *Phys. Rev. X* **10**, 041006 (2020).
- [15] V. Leeb, K. Polyudov, S. Mashhadi, S. Biswas, R. Valentí, M. Burghard, and J. Knolle, Anomalous Quantum Oscillations in a Heterostructure of Graphene on a Proximate Quantum Spin Liquid, *Phys. Rev. Lett.* **126**, 097201 (2021).
- [16] B. Sbierski, E. J. Dresselhaus, J. E. Moore, and I. A. Gruzberg, Criticality of Two-Dimensional Disordered Dirac Fermions in the Unitary Class and Universality of the Integer Quantum Hall Transition, *Phys. Rev. Lett.* **126**, 076801 (2021).
- [17] L. Guo, Y. Yan, R. Xu, J. Li, and C. Zeng, Zero-Bias Conductance Peaks Effectively Tuned by Gating-Controlled Rashba Spin-Orbit Coupling, *Phys. Rev. Lett.* **126**, 057701 (2021).
- [18] J. Bouaziz, H. Ishida, S. Lounis, and S. Blügel, Transverse Transport in Two-Dimensional Relativistic Systems with Non-trivial Spin Textures, *Phys. Rev. Lett.* **126**, 147203 (2021).
- [19] H. Rostami and E. Cappelluti, Many-body effects in third harmonic generation of graphene, *Phys. Rev. B* **103**, 125415 (2021).
- [20] B. N. Narozhny, I. V. Gornyi, and M. Titov, Hydrodynamic collective modes in graphene, *Phys. Rev. B* **103**, 115402 (2021).
- [21] J. Friedel, *Philos. Mag.* **43**, 153 (1952).
- [22] G. H. Chen and M. E. Raikh, Small- q anomaly in the dielectric function and high-temperature oscillations of the screening potential in a two-dimensional electron gas with spin-orbit coupling, *Phys. Rev. B* **59**, 5090 (1999).
- [23] V. V. Cheianov and V. I. Fal'ko, Friedel Oscillations, Impurity Scattering, and Temperature Dependence of Resistivity in Graphene, *Phys. Rev. Lett.* **97**, 226801 (2006).
- [24] A. M. Rudin, I. L. Aleiner, and L. I. Glazman, Tunneling zero-bias anomaly in the quasiballistic regime, *Phys. Rev. B* **55**, 9322 (1997).
- [25] G. Zala, B. N. Narozhny, and I. L. Aleiner, Interaction corrections at intermediate temperatures: Magnetoresistance in a parallel field, *Phys. Rev. B* **65**, 020201(R) (2001).
- [26] Gábor Zala, B. N. Narozhny, and I. L. Aleiner, Interaction corrections at intermediate temperatures: Longitudinal conductivity and kinetic equation, *Phys. Rev. B* **64**, 214204 (2001).
- [27] Gábor Zala, B. N. Narozhny, and I. L. Aleiner, Interaction corrections to the Hall coefficient at intermediate temperatures, *Phys. Rev. B* **64**, 201201(R) (2001).
- [28] K. Nomura and A. H. MacDonald, Quantum Transport of Massless Dirac Fermions, *Phys. Rev. Lett.* **98**, 076602 (2007).
- [29] E. Mariani, L. I. Glazman, A. Kamenev, and F. von Oppen, Zero-bias anomaly in the tunneling density of states of graphene, *Phys. Rev. B* **76**, 165402 (2007).
- [30] G. F. Giuliani and J. J. Quinn, Lifetime of a quasiparticle in a two-dimensional electron gas, *Phys. Rev. B* **26**, 4421 (1982).
- [31] T. Jungwirth and A. H. MacDonald, Electron-electron interactions and two-dimensional–two-dimensional tunneling, *Phys. Rev. B* **53**, 7403 (1996).
- [32] L. Zheng and S. Das Sarma, Coulomb scattering lifetime of a two-dimensional electron gas, *Phys. Rev. B* **53**, 9964 (1996).
- [33] A. V. Chubukov and D. L. Maslov, Nonanalytic corrections to the Fermi-liquid behavior, *Phys. Rev. B* **68**, 155113 (2003).

- [34] S. Misawa, Temperature-squared term in the heat capacity of a two-dimensional Fermi liquid, *J. Phys. Soc. Jpn.* **68**, 2172 (1999).
- [35] D. Coffey and K. S. Bedell, Nonanalytic Contributions to the Self-Energy and the Thermodynamics of Two-Dimensional Fermi Liquids, *Phys. Rev. Lett.* **71**, 1043 (1993).
- [36] S. Das Sarma, E. H. Hwang, and W. K. Tse, Many-body interaction effects in doped and undoped graphene: Fermi liquid versus non-Fermi liquid, *Phys. Rev. B* **75**, 121406(R) (2007).
- [37] T. A. Sedrakyán, E. G. Mishchenko, and M. E. Raikh, Smearing of the Two-Dimensional Kohn Anomaly in a Nonquantizing Magnetic Field: Implications for Interaction Effects, *Phys. Rev. Lett.* **99**, 036401 (2007).
- [38] T. A. Sedrakyán and M. E. Raikh, Crossover from Weak Localization to Shubnikov–de Haas oscillations in a High-Mobility 2D Electron Gas, *Phys. Rev. Lett.* **100**, 106806 (2008).
- [39] T. A. Sedrakyán and M. E. Raikh, Magneto-Oscillations Due to Electron-Electron Interactions in the ac Conductivity of a Two-Dimensional Electron Gas, *Phys. Rev. Lett.* **100**, 086808 (2008).
- [40] K. Wang, M. E. Raikh, and T. A. Sedrakyán, Persistent Friedel oscillations in graphene due to a weak magnetic field, *Phys. Rev. B* **103**, 085418 (2021).
- [41] To visualize the chiral symmetry breaking around a single valley, we consider the (pseudo)spin vector, $\mathbf{v}_Q(\mathbf{r})$, of the wave function at $Q = K$ or K' , defined as follows: we take the positive eigenstate $\psi(\mathbf{r})$ of the matrix M in Eq. (3), and project $\psi(\mathbf{r})$ into K valley (or K' valley) as $\psi_K(\mathbf{r})$ and then define $\mathbf{v}_K(\mathbf{r}) = \langle \psi_K(\mathbf{r}) | (\hat{\sigma}_x, \hat{\sigma}_y, \hat{\sigma}_z) | \psi_K(\mathbf{r}) \rangle$. Since the chiral transformation connects the two valleys (as shown in Fig. 1), the spin vectors at K, K' points satisfy the property $\mathbf{v}_{K'}(\mathbf{r}) = \mathbf{v}_K(-\mathbf{r})$. In Fig. 1, we plotted the vector $\mathbf{v}_K(\mathbf{r})$ to illustrate the effect of chiral-symmetry breaking around $Q = K$.
- [42] See Supplemental Material at <http://link.aps.org/supplemental/10.1103/PhysRevB.104.L161102> for all details of the calculations of the reported field-induced interaction effects.
- [43] S. Marchini, S. Günther, and J. Wintterlin, Scanning tunneling microscopy of graphene on Ru(0001), *Phys. Rev. B* **76**, 075429 (2007).
- [44] G. H. Li, A. Luican, and E. Y. Andrei, Scanning Tunneling Spectroscopy of Graphene on Graphite, *Phys. Rev. Lett.* **102**, 176804 (2009).
- [45] B. Lv, T. Qian, and H. Ding, Angle-resolved photoemission spectroscopy and its application to topological materials, *Nat. Rev. Phys.* **1**, 609 (2019).
- [46] M. Mucha-Kruczyński, O. Tsypliyatyev, A. Grishin, E. McCann, V. I. Fal'ko, A. Bostwick, and E. Rotenberg, Characterization of graphene through anisotropy of constant-energy maps in angle-resolved photoemission, *Phys. Rev. B* **77**, 195403 (2008).
- [47] Q. Li, K. Xia, J. Zhang, Y. Zhang, Q. Li, K. Takahashi, and X. Zhang, Measurement of specific heat and thermal conductivity of supported and suspended graphene by a comprehensive Raman optothermal method, *Nanoscale* **9**, 10784 (2017).
- [48] A. Sedrakyán, A. Sinner, and K. Ziegler, Deformation of a graphene sheet: Interaction of fermions with phonons, *Phys. Rev. B* **103**, L201104 (2021).
- [49] C. Faugeras, P. Kossacki, D. M. Basko, M. Amado, M. Sprinkle, C. Berger, W. A. de Heer, and M. Potemski, Effect of a magnetic field on the two-phonon Raman scattering in graphene, *Phys. Rev. B* **81**, 155436 (2010).
- [50] M. Kharitonov, Phase diagram for the $\nu = 0$ quantum Hall state in monolayer graphene, *Phys. Rev. B* **85**, 155439 (2012).
- [51] M. O. Goerbig, Electronic properties of graphene in a strong magnetic field, *Rev. Mod. Phys.* **83**, 1193 (2011).